CHALMERS

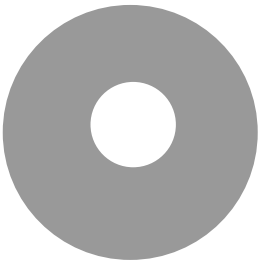

Characterization of an integrating sphere radiation reference source

Master of Science Thesis

VICTOR SANDGREN

Department of Signals and Systems
Division of Signal Processing and Biomedical Engineering
CHALMERS UNIVERSITY OF TECHNOLOGY
Göteborg, Sweden 2011
Report No. EX084/2011

REPORT NO. EX084/2011

Characterization of an integrating sphere radiation reference source

Master of Science Thesis
VICTOR SANDGREN

Department of Signals and Systems
Division of Signal Processing and Biomedical Engineering
CHALMERS UNIVERSITY OF TECHNOLOGY

Göteborg, Sweden 2011

Characterization of an integrating sphere
radiation reference source
VICTOR SANDGREN

Report No. EX084/2011
Department of Signals and Systems
Division of Signal Processing and Biomedical Engineering
Chalmers University of Technology
SE-412 96 Göteborg
Sweden
Telephone: + 46 (0)31-772 1000

Cover:
Integrating sphere, artist's impression.

Chalmers Reproservice
Göteborg, Sweden 2011

Characterization of an integrating sphere
radiation reference source
Master of Science Thesis
VICTOR SANDGREN
Department of Signals and Systems
Division of Signal Processing and Biomedical Engineering
Chalmers University of Technology

Abstract

To test and characterize imaging systems there is often a need for a source that can provide uniform radiation in the desired wavelength band. An integrating sphere is an optical instrument that is often used as a source of uniform radiation in the visible and near-infrared spectra. In this work an integrating sphere constructed at the Swedish Defence Research Agency in Linköping is characterized regarding spectral radiance and luminance uniformity. The spectral radiance is measured with a spectrometer in the wavelength interval from 300 nm to 1000 nm and with a broadband detector in the intervals from 1.46 µm to 1.79 µm and 2.13 µm to 2.57 µm. The luminance is mapped with a luminance meter giving a uniformity of 95.4%. Some additional uniformity measurements are made with a DSLR-camera indicating that the luminance is considerably lower for large fields of view into the sphere.

Keywords: integrating sphere, uniform light source, radiometry

Contents

Preface

This work was carried out at the Swedish Defence Research Agency, FOI, in Linköping, Sweden, from March to August 2011 with Ph.D. Thomas Svensson as supervisor. Examiner has been professor Mikael Persson at Chalmers University of Technology.

Acknowledgements

The author would like to thank a number of people for their contributions to this work. Thomas Svensson. Roland Lindell and Ingmar Renhorn at FOI, Mikael Persson and Artur Chodorowski at Chalmers, and last but not least Mr. Debdeep Ray for his review of the thesis.

Göteborg September 2011
Victor Sandgren

1 Introduction

1.1 Background

In the characterization of imaging systems parameters such as the linearity and uniformity of the sensor array as well as distortions introduced by the optical components are of interest. To detect non-uniformities in the sensor array sensitivity, figure 1.1, and distortions such as vignetting and narcissus effects, figure 1.2, introduced by the optics, a reference source, that can supply the system with uniform radiation of a suitable wavelength is needed. If the linearity is to be measured the radiation level of the source should ideally cover the entire dynamic range of the sensor. At long wavelengths blackbody sources, such as a plate held at uniform temperature, are often used as reference sources. For wavelengths shorter than about 3 µm the required temperatures render this solution impractical. An alternative solution for shorter wavelengths is to use an integrating sphere, sometimes called an Ulbricht sphere. These are available commercially but tend to become very expensive for large sizes. At the Swedish Defence Research Institute, FOI, an integrating sphere with a diameter of 60 cm has been constructed to be used as a short wave radiation reference source. More on the topic of imaging system characterization can be found in [1].

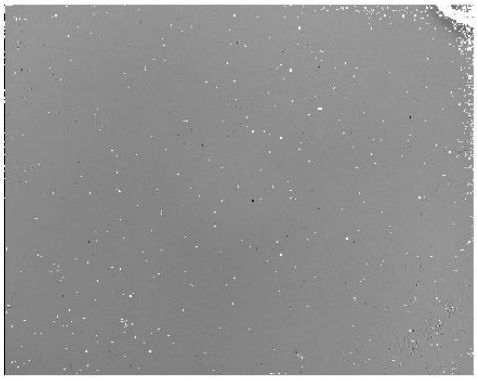

Figure 1.1: Image of a black body radiator acquired with an infrared camera. The image contains both temporal noise and fixed pattern noise due to non-uniformity of sensor array.

1.2 Purpose

The purpose of this project is to characterize the integrating sphere constructed at FOI and assess its potential as a reference source. The primary quantities of interest are the uniformity of the radiation and the spectral distribution in the visual and near-infrared regions.

1.3 Limitations

To completely specify the uniformity of the sphere, the radiation would need to be measured in all directions for every point at the exit port surface. In this work mostly directions near normal to the port are considered, corresponding to small fields of view of the instrument under test. Furthermore the uniformity is only measured in the visible spectrum though it might vary somewhat with the wavelength.

Figure 1.2: Infrared areal image, the dark spot in the center of the image is due to narcissus effect. Unintended reflections inside the instrument causes the sensor to see itself as a cold spot.

1.4 Approach

The uniformity was measured by mapping the luminance at the exit port using a commercial luminance meter. Some additional uniformity measurements were made with a DSLR-camera. The spectral distribution was measured with a spectrometer in the wavelength interval from 300 to 1000 nm and with a broadband meter in the intervals from 1.46 µm to 1.79 µm and 2.13 µm to 2.40 µm, respectively.

1.5 Thesis overview

The following chapter, 2, goes through some radiometric and photometric concept used in the rest of the thesis. The reader familiar with radiometry might well skip this and the sane reader might well skip the subsequent chapters as well. Chapter 3 contains a short summary of the theory behind integrating spheres. Chapter 4 describes the sphere constructed at FOI. A description of the measurement equipment used is found in chapter 5. Chapter 6 contains the results from the measurements and chapter 7 some conclusions and recommendations for future work. An introduction to solid angles can be found in an appendix.

2 Some radiometric and photometric concepts

Radiometry and photometry deal with the measurement of electromagnetic radiation. In radiometry the radiation is measured in terms of absolute power while photometry is concerned with the stimulus it has on the human eye. In this section some radiometric and photometric quantities and concepts used in the thesis are described. Some elementary knowledge of geometrical optics is assumed, the reader unfamiliar with this can consult e.g. [2].

2.1 Radiometric and photometric quantities

The radiometric and photometric quantities introduced in this section are listed in table 2.1. Subscript e denotes radiometric quantities and subscript v photometric ones. In the rest of the text the subscripts are sometimes omitted if it is clear from the context what is meant, or if the relations are valid for both the radiometric and the corresponding photometric quantity. The disposition follows that in [3], introducing radiance as the basic radiometric quantity.

Table 2.1: Some radiometric and photometric quantities.

Radiometric quantity	Symbol	SI-units
Radiant flux	Φ_e	W
Radiance	L_e	$\mathrm{W} \cdot \mathrm{m}^{-2} \cdot \mathrm{sr}^{-1}$
Radiant exitance	M_e	$\mathrm{W} \cdot \mathrm{m}^{-2}$
Irradiance	E_e	$\mathrm{W} \cdot \mathrm{m}^{-2}$
Radiant intensity	I_e	$\mathrm{W} \cdot \mathrm{sr}^{-1}$
Spectral radiometric quantity	**Symbol**	**SI-units**
Spectral radiant flux	$\Phi_{e,\lambda}$	$\mathrm{W} \cdot \mathrm{nm}^{-1}$
Spectral radiance	$L_{e,\lambda}$	$\mathrm{W} \cdot \mathrm{m}^{-2} \cdot \mathrm{sr}^{-1} \cdot \mathrm{nm}^{-1}$
Spectral radiant exitance	$M_{e,\lambda}$	$\mathrm{W} \cdot \mathrm{m}^{-2} \cdot \mathrm{nm}^{-1}$
Spectral irradiance	$E_{e,\lambda}$	$\mathrm{W} \cdot \mathrm{m}^{-2} \cdot \mathrm{nm}^{-1}$
Spectral radiant intensity	$I_{e,\lambda}$	$\mathrm{W} \cdot \mathrm{sr}^{-1} \cdot \mathrm{nm}^{-1}$
Photometric quantity	**Symbol**	**SI-units**
Luminous flux	Φ_v	lm
Luminance	L_v	$\mathrm{lm} \cdot \mathrm{m}^{-2} \cdot \mathrm{sr}^{-1}$
Luminous exitance	M_v	$\mathrm{lm} \cdot \mathrm{m}^{-2}$
Illuminance	E_v	$\mathrm{lm} \cdot \mathrm{m}^{-2}$
Luminous intensity	I_v	$\mathrm{lm} \cdot \mathrm{sr}^{-1}$

Radiance Consider a ray of radiation leaving a surface at a point P (figure 2.1). The radiance at P in the direction of the ray is defined as [4]

$$L_e = \lim_{\Delta A, \Delta\omega \to 0} \frac{\Delta \Phi_e}{\Delta A \cos\theta \Delta\omega} = \frac{d^2\Phi_e}{dA \cos\theta d\omega}, \tag{2.1}$$

where $\Delta\Phi_e$ is the radiant flux leaving ΔA within the solid angle $\Delta\omega$ and θ is the angle between the ray and the surface normal. The same definition holds for radiation incident upon, or passing through a (virtual) surface. In general the radiance is a function of both

position on the surface and direction, $L_e = L_e(x, y, \theta, \phi)$.[1] The term $\Delta A \cos\theta$ is the area ΔA projected onto a plane perpendicular to the ray. This is the effective area seen by an observer positioned in the direction of the ray, the radiance is therefore a measure of the perceived brightness of a surface.[2] From the definition radiance has units of radiant flux per unit projected area and per unit soild angle, $[\mathrm{W} \cdot \mathrm{m}^{-2} \cdot \mathrm{sr}^{-1}]$.

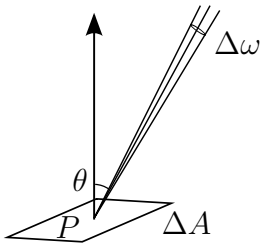

Figure 2.1: Ray leaving a surface.

Radiant exitance and irradiance Rearranging (2.1) yields

$$d^2\Phi_e = L_e \cos\theta \, dA \, d\omega. \tag{2.2}$$

Dividing by dA and integrating over a solid angle ω gives the flux per unit area within that solid angle,

$$\frac{d\Phi_e}{dA} = \int_\omega L_e \cos\theta \, d\omega. \tag{2.3}$$

Integrating over the entire hemisphere above some point in a surface yields the total flux per unit area incident upon, or emerging from, the surface at that point, regardless of direction. This quantity is usually called radiant exitance or radiant emittance, M_e, if the radiation is leaving the surface and irradiance, E_e, if the radiation is toward the surface. It has units of radiant flux per unit area, $[\mathrm{W} \cdot \mathrm{m}^{-2}]$.

Radiant intensity If (2.2) is divided by $d\omega$ and integrated over a surface it gives the flux per unit solid angle from the entire surface in a given direction. The resulting quantity is called the radiant intensity, I_e, and is normally only applied to point sources. It has units of radiant flux per unit solid angle, $[\mathrm{W} \cdot \mathrm{sr}^{-1}]$.

Radiant flux The total radiant flux, Φ_e, incident upon, emerging from, or passing through a, real or imaginary, surface, A, within a solid angle, ω, is obtained by integrating (2.2) with respect to both solid angle and area,

$$\Phi_e = \int_A \int_\omega L_e \cos\theta \, d\omega \, dA. \tag{2.4}$$

[1] Note that the angle θ represents both the direction of the ray in a spherical coordinate system and the angle between the ray and the surface normal. These are the same only if the surface normal is in the zenith direction of the coordinate system. In the rest of the text this will always be the case.

[2] If the observer is human it is rather the luminance, described below, that measures the perceived brightness.

Spectral radiance The spectral radiance is given by

$$L_{e,\lambda} = \lim_{\Delta\lambda \to 0} \frac{\Delta L_e}{\Delta \lambda} = \frac{dL_e}{d\lambda}, \tag{2.5}$$

where ΔL_e is the radiance in the wavelength interval $\Delta\lambda$. It has units of radiance per unit wavelength, $[\mathrm{W} \cdot \mathrm{m}^{-2} \cdot \mathrm{sr}^{-1} \cdot \mathrm{nm}^{-1}]$. Spectral radiance can also be defined with respect to frequency or wavenumber. Spectral forms of exitance, irradiance, radiant intensity and radiant flux are defined in a similar way.

Photometric quantities Modifying the above radiometric quantities, so that they take the response of the human eye to the radiation into account, gives the corresponding photometric ones. The photometric equivalent to radiant flux is called luminous flux and has the unit lumen [lm]. It is given by

$$\Phi_v = K_m \int_{360nm}^{830nm} \Phi_{e,\lambda} V(\lambda)\, d\lambda. \tag{2.6}$$

$K_m \approx 683$ lm/W is the *maximum spectral luminous efficacy* and $V(\lambda)$ is the *photopic luminous efficiency function*, standardized by CIE [5]. $V(\lambda)$ has a maximum value of 1 at 550 nm where the human eye is most sensitive, see figure 2.2.

The photometric equivalent to radiance is called luminance, L_v, and has units luminous flux per unit area and unit solid angle, $[\mathrm{lm} \cdot \mathrm{m}^{-2} \cdot \mathrm{sr}^{-1}]$. Luminous exitance (emittance), M_v and Illuminance, E_v correspond to radiant excitance and irradiance, respectively. Both have units luminous flux per unit area, $[\mathrm{lm} \cdot \mathrm{m}^{-2}]$. Luminous intensity, I_v corresponds to radiant intensity and has units luminous flux per unit solid angle, $[\mathrm{lm} \cdot \mathrm{sr}^{-1}]$. Lumens per steradian has been given the SI-unit candela, [cd], which is one of the basic SI-units. Consequently luminance can be measured in cd/m^2 as well.

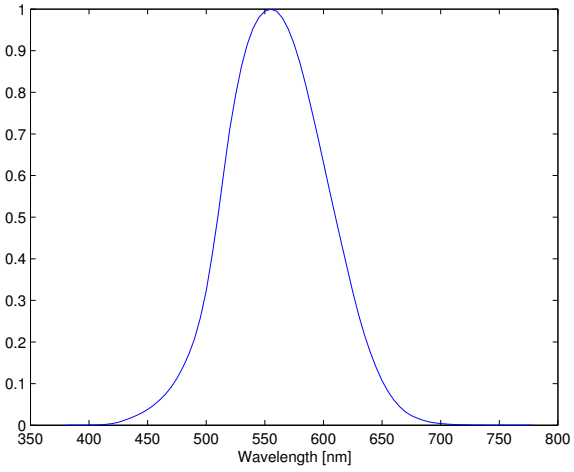

Figure 2.2: Graph of the photopic luminous efficiency function, $V(\lambda)$.

2.2 Lambertian surfaces

A radiating surface is said to be perfectly diffuse, or Lambertian, if the radiation follows *Lambert's cosine law*. This says that the radiant intensity from the surface in a given direction should be proportional to the cosine of the angle to the surface normal. Consequently the radiance from the surface is isotropic. The radiation can be reflected, emitted

or passing through a virtual surface. A Lambertian reflecting surface that is uniformly irradiated becomes an *iso-radiance* source, with constant radiance at all points and in all directions.

For a Lambertian surface (2.3) gives

$$M = \int_\omega L\cos\theta\, d\omega = L\int_0^{2\pi}\int_0^{\frac{\pi}{2}} \cos\theta\sin\theta\, d\theta\, d\phi = \pi L, \tag{2.7}$$

where ω is the hemisphere above the surface and $\sin\theta\, d\theta\, d\phi$ is the element of solid angle, $d\omega$, in spherical coordinates, (A.1).

2.3 Radiation exchange and configuration factors

2.3.1 Radiation exchange between differential elements

Figure 2.3 shows two area elements joined by a line of length S, making angles θ_1 and θ_2 with the surface normals. The flux incident on dA_2 from dA_1 is

$$d^2\Phi_{d1-d2} = L_{d1-d2}\cos\theta_1 dA_1 d\omega_2 = L_{d1-d2}\frac{\cos\theta_1\cos\theta_2}{S^2}dA_1 dA_2, \tag{2.8}$$

where L_{d1-d2} is the radiance of dA_1 in the direction of dA_2 and $d\omega_2 = dA_2\cos\theta_2/S^2$ is the solid angle subtended by dA_2 at dA_1.[3] If dA_1 is Lambertian it has a constant radiance, L_1, over the hemisphere containing dA_2 and the total flux from dA_1 into the hemisphere is $d\Phi_1 = \pi L_1 dA_1$. The fraction of flux from dA_1 incident on dA_2 is called the *configuration factor* [6]

$$dF_{d1-d2} = \frac{\cos\theta_1\cos\theta_2}{\pi S^2}dA_2. \tag{2.9}$$

The flux from dA_1 to dA_2 can now be calculated as

$$d^2\Phi_{d1-d2} = \pi L_1 dA_1 dF_{d1-d2}. \tag{2.10}$$

Reversing the roles of dA_1 and dA_2 yields

$$dF_{d2-d1} = \frac{\cos\theta_1\cos\theta_2}{\pi S^2}dA_1 \tag{2.11}$$

and the relation

$$dF_{d1-d2}dA_1 = dF_{d2-d1}dA_2. \tag{2.12}$$

2.3.2 Radiation exchange between circular disc and differential element

A differential element parallel to a circular disc, positioned along the normal through the center of the disc, is shown in figure 2.4. Assume the surfaces to be Lambertian with radiance L_{d1} and L_2, respectively. The flux from dA_1 to A_2 is now given by

$$d\Phi_{d1-2} = L_{d1}dA_1\int_\omega \cos\theta d\omega = L_{d1}dA_1\int_0^{2\pi}\int_0^{\alpha}\cos\theta\sin\theta\, d\theta\, d\phi = \pi L_{d1}dA_1\sin^2\alpha. \tag{2.13}$$

The flux from dA_1 into the hemisphere is $d\Phi_{d1} = \pi L_{d1}dA_1$ and the configuration factor becomes

$$F_{d1-2} = \sin^2\alpha = \frac{r^2}{h^2+r^2}. \tag{2.14}$$

[3] Following [6] the subscript $d1-d2$ on a quantity means that it is from a differential area 1 to a differential area 2. For finite areas the d is omitted, thus $d\Phi_{d1-2}$ indicates the element of flux from a differential area 1 to a finite area 2.

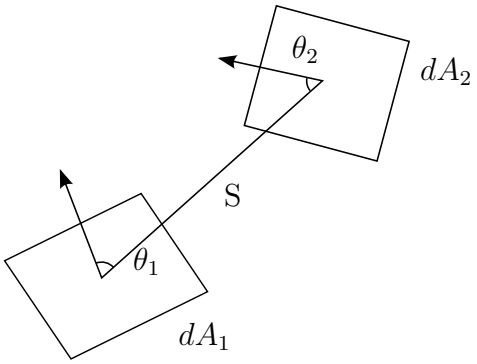

Figure 2.3: Two differential surface elements exchanging radiation.

To get the flux from A_2 to dA_1, L_{d1} is replaced with L_2 in (2.13) giving

$$d\Phi_{2-d1} = \pi L_2 dA_1 \frac{r^2}{h^2 + r^2}. \tag{2.15}$$

The flux from A_2 into the hemisphere is $\Phi_2 = \pi L_2 A_2$ resulting in

$$dF_{2-d1} = \frac{dA_1}{A_2} \frac{r^2}{h^2 + r^2}. \tag{2.16}$$

Combining (2.14) and (2.16) gives the relation

$$F_{d1-2} dA_1 = dF_{2-d1} A_2, \tag{2.17}$$

which holds in general for configuration factors between a differential and a finite area, see [6].

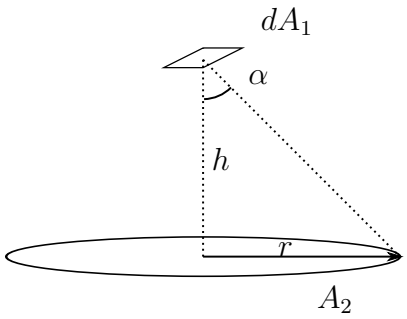

Figure 2.4: Disc and differential area element exchanging radiation. Area element on normal through disc center and parallel to disc.

For many common situations configuration factors can be found in tables. In the case where the differential element is not located on the normal through the center of the disc, see figure 2.5, the configuration factor can be found in [6] to be

$$F_{d1-2} = \frac{1}{2}\left(1 - \frac{1 + H^2 - R^2}{\sqrt{Z^2 - 4R^2}}\right), \tag{2.18}$$

where $H = h/a$, $R = r/a$ and $Z = 1 + H^2 + R^2$.

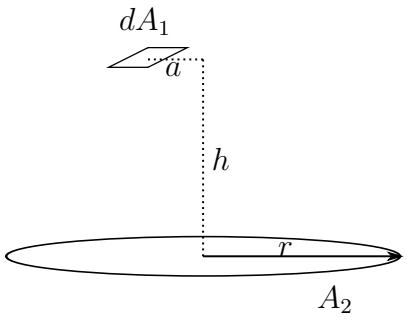

Figure 2.5: Disc and differential area element exchanging radiation. Area element parallel to disc.

2.4 Radiance invariance

Consider again the two differential area elements in figure 2.3. The element of flux from dA_1 in the direction of dA_2 is

$$d^2\Phi_{d1-d2} = L_{d1-d2} dA_1 \cos\theta_1 \frac{dA_2 \cos\theta_2}{S^2} \tag{2.19}$$

where L_{d1-d2} is the radiance leaving dA_1 in the direction of dA_2. The element of flux incident on dA_2 from the direction of dA_1 is

$$d^2\Phi'_{d2-d1} = L'_{d2-d1} dA_2 \cos\theta_2 \frac{dA_1 \cos\theta_1}{S^2} \tag{2.20}$$

with L'_{d2-d1} being the radiance incident on dA_2 from the direction of dA_1. If there is no losses in the medium between dA_1 and dA_2, $d^2\Phi_{d1-d2}$ is equal to $d^2\Phi'_{d2-d1}$ and consequently $L_{d1-d2} = L'_{d2-d1}$. The *elementary beam* between dA_1 and dA_2 consists of all rays between the two area elements. From the above it can be seen that radiance is constant along such a beam if no losses are present. A perfect radiance (or luminance) meter pointed at a radiating object along some ray will therefore give the same reading regardless of the distance from the object.

2.5 Field of view and F-number

Figure 2.6 shows a simple radiation meter consisting of a lens and a single detector element. The size of the sensor and its distance to the lens determines the *field of view*, α, of the meter. If the detector element is not circular the field of view depends on in which plane, containing the optical axis, it is measured.

In an imaging system the sensor consists of an array of detector elements. The field of view of an imaging system usually refers to that of the entire sensor, while that of a single detector element is called the instantaneous field of view.

When the detector is focused on a radiating object the amount of flux that reaches the detector depends on the area, A, of the object that falls within the field of view, the solid angle, ω, subtended by the lens at the object and the radiance, L, of the object. If the lens is assumed to be lossless the flux on the detector is

$$\Phi = \int_A \int_\omega L \cos\theta d\omega dA \tag{2.21}$$

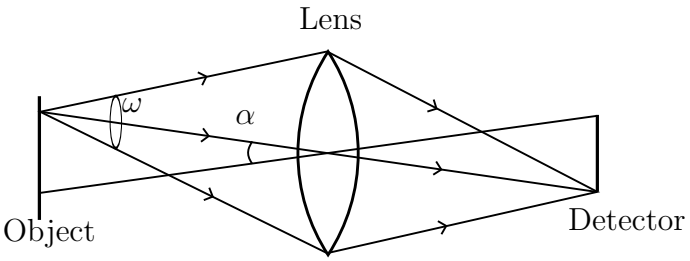

Figure 2.6: A simple radiation meter

where θ is the angle to the surface normal of the object. For a Lambertian surface L can be moved outside the integral yielding

$$\Phi = L \int_A \int_\omega \cos\theta d\omega dA \tag{2.22}$$

or

$$\Phi = \pi L A F_{1-2} \tag{2.23}$$

where F_{1-2} is the configuration factor from the area seen by the detector to the lens.

A larger lens collects the radiation over a larger solid angle and increases the flux received by the detector. In most optical systems the flux is not received over the entire lens but is limited by an aperture stop. In this case it is the solid angle subtended by the aperture stop that determines the flux received by the detector. If there are lenses in front of the aperture stop it is instead the *entrance pupil*, which is the image of the aperture stop seen from the radiating object, that determines how much flux is gathered by the instrument. The *relative aperture* or *f-number*, F, of an optical system is defined as

$$F = f/D \tag{2.24}$$

where f is the effective focal length and D is the diameter of the entrance pupil. For a fixed focal length a low f-number indicates a large entrance pupil and the system gathers flux over a large solid angle. The f-number stated on photographic lenses and other optical instruments is usually calculated when the instrument is focused at infinity. An f-number of e.g. $F = 8$ is often written as $f/8$.

2.6 Measuring radiation with broadband detectors

The output signal from a radiation detector can typically be written on the form

$$S = \int_0^\infty \Phi_{e,\lambda} R(\lambda) d\lambda, \tag{2.25}$$

where S is the output signal, $\Phi_{e,\lambda}$ the spectral radiant flux incident upon the detector and R is the response function of the detector. In general R can be a function of several variables but only the wavelength dependency will be of interest here. The units of R must match S, if e.g. the output signal is in volts, R will have units of $[V/W]$. Often a filter is used in conjunction with the detector in which case the relation becomes

$$S = \int_0^\infty \Phi_{e,\lambda} R(\lambda) \tau(\lambda) d\lambda, \tag{2.26}$$

with τ being the transmittance of the filter. In some cases an additional term is included to account for the dark signal of the detector. For an ideal detector, R (or the product $R \cdot \tau$), would be constant over some wavelength band of interest and zero outside. In real detectors the value of R can vary considerably over the range of the detector. If two measurements are to be comparable, when R is non-constant, the sources in the measurements must have the same relative spectral distribution. If the spectral distribution of the sources are different they can result in different signals from the detector, even if they deliver the same total flux in the measured wavelength band. Though it is hard to manufacture detectors with a flat response curve, detectors can be made that follow the photopic luminous efficiency function closely. Thus, the spectral distribution of the source is usually not very important when photometric quantities are measured.

3 Integrating sphere theory

An integrating sphere consists in its simplest form of a spherical enclosure coated on the inside with some reflecting material and a number of ports to let radiation in and out. In this section some equations are derived for an integrating sphere when the coating is a Lambertian reflector and the ports have zero reflectance. Similar derivations can be found in [7] and [8].

3.1 Radiation exchange in a diffusely reflecting sphere

From (2.9) the configuration factor for two differential elements is

$$dF_{d1-d2} = \frac{\cos\theta_1 \cos\theta_2}{\pi S^2} dA_2, \tag{3.1}$$

where S is the length of the line connecting the elements and θ_1 and θ_2 are the angles between that line and the surface normals. When the surface elements lie on the inside of a sphere of radius R (figure 3.1), $\cos\theta_1 = \cos\theta_2 = S/2R$ and

$$dF_{d1-d2} = \frac{dA_2}{4\pi R^2}. \tag{3.2}$$

Since this is independent of the positions of the two surface elements the flux from any point on the sphere surface is distributed uniformly over the entire sphere. The flux received by a finite area A_2 is

$$\Phi_1 \frac{A_2}{A_s}$$

where A_s is the surface area of the entire sphere.

When a beam of light is incident on the sphere wall it will be uniformly distributed over the entire wall after the first reflection. The portion of the sphere wall that has only received reflected light will thus have constant radiance. If a portion of the wall is replaced by an exit port, shielded from unreflected light, it can be seen as a virtual iso-radiance surface.

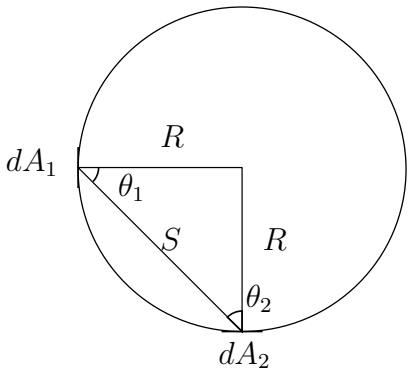

Figure 3.1: Surface elements inside sphere.

3.2 Multiple reflections and the sphere multiplier

When the sphere is illuminated by an external source the radiation will be reflected multiple times from the sphere surface and some of it will be lost through the ports, both entrance and exit ports are assumed to have zero reflectance. If ρ is the reflectance of the sphere

wall and f is the port fraction, i.e. the fraction of the sphere surface area occupied by the ports, the flux incident on the sphere wall after the first reflection is

$$\Phi_i \rho (1 - f)$$

where Φ_i is the flux from the entrance port. After n reflections the incident flux will be

$$\Phi_i \rho^n (1 - f)^n.$$

The total incident flux after an infinite number of reflections becomes

$$\Phi_i \rho (1 - f) \sum_{n=0}^{\infty} \rho^n (1 - f)^n = \frac{\Phi_i \rho (1 - f)}{1 - \rho(1 - f)}.$$

Since the sphere wall is assumed to be Lambertian the radiance is given by

$$L_w = \frac{\Phi_i}{\pi A_s (1 - f)} \cdot \frac{\rho(1 - f)}{1 - \rho(1 - f)} = \frac{\Phi_i}{\pi A_s} \cdot M \tag{3.3}$$

where $M = \rho/(1 - \rho(1 - f))$ is called the sphere multiplier [7]. The sphere multiplier is a measure of how much higher the radiance of the sphere wall is, due to multiple reflections, compared to the case when the same amount of flux is reflected from a flat surface of the same area. It can be seen that the wall radiance decreases with increasing sphere size for a fixed value of M and that M increases with increasing wall reflectance and decreasing port fraction. For $\rho = 1$ we get

$$L_w = \frac{\Phi_i}{\pi A_s} \cdot \frac{1}{f} \tag{3.4}$$

and the flux out of the ports is

$$\Phi_o = \pi A_s f \cdot L = \Phi_i \tag{3.5}$$

as expected. In general the reflectance is a function of wavelength and so is the sphere multiplier, $M = M(\lambda)$.

The area, A_i, of the sphere wall on which the incoming flux is incident will have an average radiance

$$L_i = \frac{\Phi_i \rho}{\pi A_i} + L_w. \tag{3.6}$$

Dividing this by L_w from equation 3.3 yields

$$\frac{L_i}{L_w} = 1 + \frac{A_s}{A_i}(1 - \rho(1 - f)) = 1 + \frac{A_s}{A_i}\frac{\rho}{M}. \tag{3.7}$$

When this area falls within the field of view of a sensor at the exit port, the radiation received by the sensor will not be uniform and it can be necessary to introduce baffles to shield the sensor from the first reflection of the incoming radiation. If the incoming radiation is spread evenly over a large area and the value of the sphere multiplier is high the problem is less severe.

Real sphere coatings are not perfectly diffuse and it is desirable to have as many reflections as possible in the sphere to make the radiation uniform. A large value of the sphere multiplier thus increases both the uniformity and the maximum radiance from the sphere. To get a large value of M a rule of thumb is to keep the port fraction below 5 % and the wall reflectance as high as possible [7, 9]. The size of the ports are often determined by the application and the total size of the sphere is adjusted to keep the port fraction reasonably low. When the sphere is used as a source of uniform radiation, the exit port size is determined by the instruments it will supply with radiation.

4 The integrating sphere at FOI

The sphere constructed at FOI consists of two connected aluminum half-spheres with an inner diameter of 60 cm. The inside is coated with a matt white paint , with a reflectance curve according to figure 4.2. Two lamp assemblies, consisting of a halogen spotlight (Osram 64634), an iris diaphragm and a diffuser glass, irradiate the sphere through two inlet ports. The lamps are fed by a current controlled power supply unit and the radiation level is varied by means of the diaphragms. An illuminance meter, Solar Light PMA2130, is placed in the sphere wall to measure the radiation level. The exit port has a diameter of 20 cm and the total port fraction is about 3.7%. From the reflectance curve of the coating and the port fraction the sphere multiplier can be calculated. It has a maximum value of 4.7 around 500 nm and a value of 2.7 at 1000 nm.

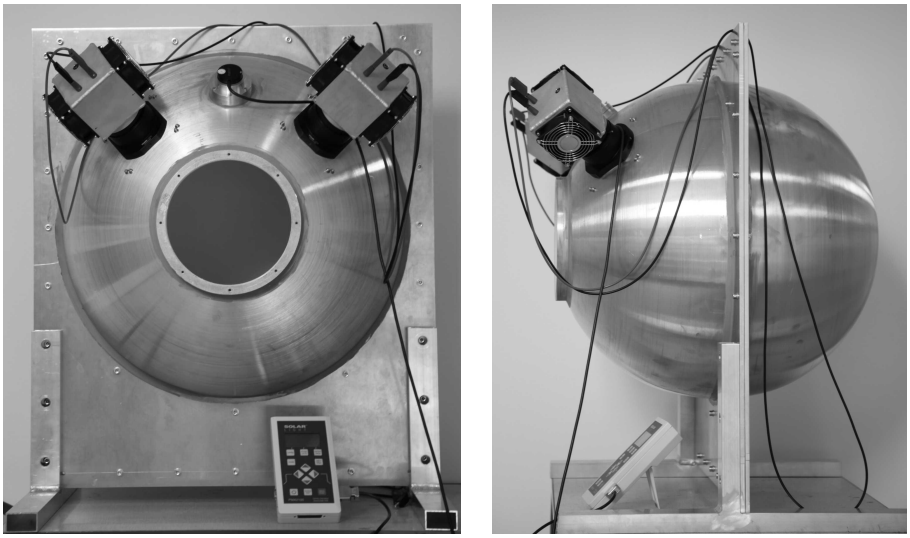

Figure 4.1: The integrating sphere constructed at FOI, front and side view, respectively.

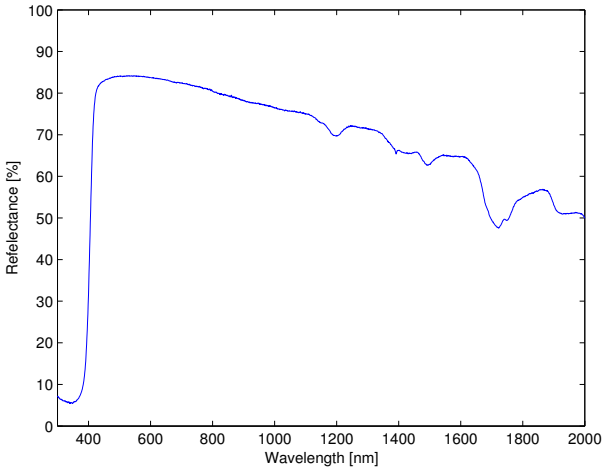

Figure 4.2: Reflectance of the sphere coating.

5 Measurement equipment

This section contains a short description of the equipment used in this thesis.

SphereOptics LR-12 H The LR-12 H is a commercially available integrating sphere from SphereOptics. The diameter of the sphere is 30.5 cm (12 in) and the exit port has a diameter of 10.2 cm (4 in). A variable attenuator is used to adjust the output luminance and the maximum luminance is about 17,000 lm. The luminance uniformity at the exit port is stated to be ±1%, or about 98% if it is measured as the ratio of lowest to highest luminance, as it will be in the following sections. An internal radiation meter calibrated to the exit port is used to read off the output luminance or spectral radiance. The sphere was used as a reference source to check some of the other equipment.

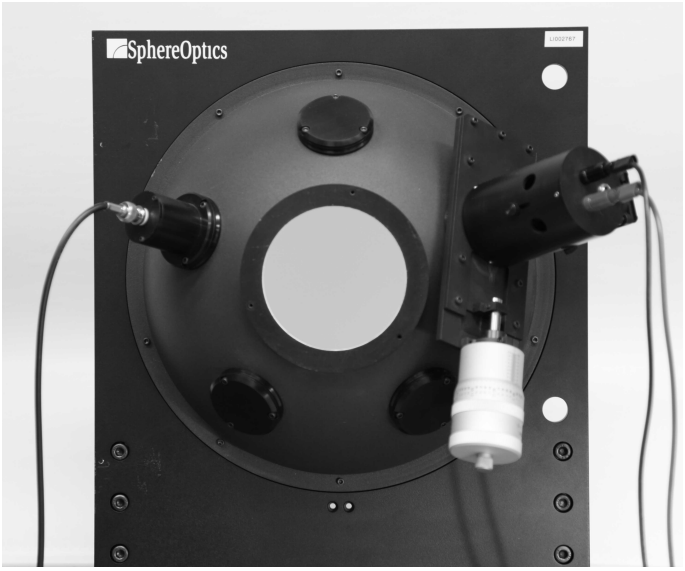

Figure 5.1: SphereOptics LR-12 H.

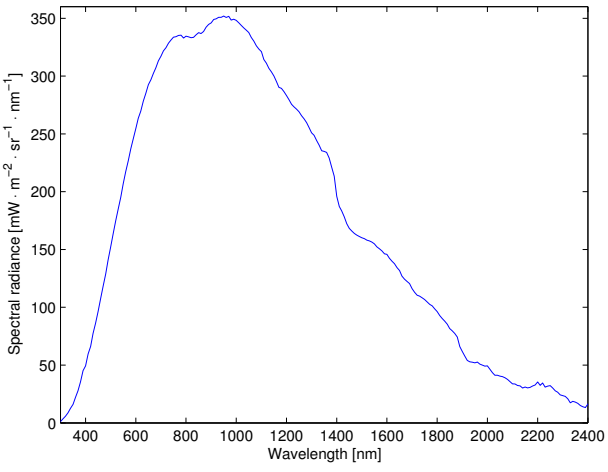

Figure 5.2: Spectral radiance, SphereOptics LR-12 H.

Minolta LM1 The Minolta LM1 is a luminance meter with a 1° acceptance angle. At the minimum distance of 1 m the measuring spot is a circle with a diameter of 15 mm. The

meter was used to map the luminance uniformity of the FOI-sphere. Because the meter was made in the seventies it was checked against the SphereOptics-sphere to make sure that it gave reasonable readings. Figure 5.4 shows a plot of the readings from the luminance meter against the readings from the sphere. Although the values from the luminance meter are about 25% lower than from the sphere the linearity seems to be good over the whole range tested. The solid line in the figure is a linear fit of the luminance meter to the sphere that has been used to rescale the readings from the luminance meter. In the luminance mapping of the FOI-sphere the relative luminance is of most interest and a small error in the absolute luminance is of less concern as long as the linearity is good.

Figure 5.3: Minolta LM1.

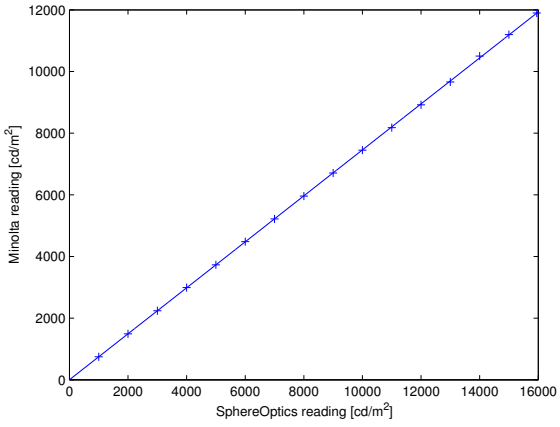

Figure 5.4: Luminance readings from Minolta LM1 against SphereOptics LR-12H, crosses. Solid line shows a linear least squares fit.

Canon EOS 5D mark II The Canon EOS 5D mark II is a digital single-lens reflex camera (DSLR) with a full-frame CMOS sensor. It was used to make additional measurements of the uniformity of the FOI-sphere, and was equipped with either a 70-200 mm or a 24-105 mm zoom lens.

Figure 5.5: Canon EOS 5D mark II.

Avantes AvaSpec-2048 Avantes AvaSpec-2048 is a fiber optic spectrometer usable in the range 200-1100 nm. The fiber end is fitted with a diffusor to collect radiation over the entire hemisphere. It is calibrated for spectral irradiance with a calibration uncertainty of 10% and a resolution of 5 nm and was used to measure the spectral radiance of the sphere from 300-1000 nm.

Figure 5.6: Avantes AvaSpec-2048.

Thorlabs PDA10DT To measure the radiance at longer wavelengths two single element detectors, PDA10DT, from Thorlabs were used. They were fitted with a 1.46-1.79 μm and a 2.13-2.57 μm filter, respectively. Tubes mounted on the detectors limited the field of view to 23.3°.

Figure 5.7: Thorlabs PDA10DT.

6 Measurement results

The uniformity of the sphere was measured by mapping the luminance with the luminance meter and some additional measurements were made with de DSLR camera. The maximum spectral radiance was measured with the Avantes spectrometer in the interval from 300 nm to 1000 nm and with the Thorlabs detectors in the intervals from 1.46 µm to 1.79 µm and 2.13 µm to 2.57 µm.

In the first measurements in the luminance mapping the lamps of the sphere were fed a constant current by the power supply. For some reason this led to quite large variations in the total radiation level, the reading on the internal illuminance meter ranged from about 12000 $\mathrm{lm/m^2}$ to 12600 $\mathrm{lm/m^2}$. In the remaining measurements the lamps were fed in series with a constant voltage of 30.5 V. After allowing the sphere to stabilize for about 10 minutes the level was now stable around 12000 $\mathrm{lm/m^2}$ with a variation of less than 1%. The effect of variations in total radiation level has been corrected for in the luminance mapping and ignored otherwise.

6.1 Uniformity

6.1.1 Luminance mapping

A first mapping of the sphere luminance was made with the luminance meter, mounted in a bracket allowing it to be translated over the exit port surface at a distance of 1 m, see figure 6.1. At this distance the measuring spot of the meter is a circle with a diameter of about 15 mm. The luminance was measured in 44 points with a separation of 25 mm as shown in figure 6.2. For each point the reading of the internal illuminance meter was recorded together with the reading of the luminance meter, so that the latter could be corrected for drifts in the overall output of the sphere. A total of five separate mappings was made of the exit port with the sphere at full power, table 6.1 shows the mean value and the standard deviation of the luminance for the 44 points. Here the reading of the luminance meter has been calibrated to the SphereOptics-sphere according to the curve in figure 5.4 and the values have been adjusted to correspond to a illuminance of 12000 lx on the internal meter of the sphere.

In table 6.2 the luminance values have been normalized to point 5 which was the brightest point. It can be seen that the lowest relative luminance is 95.4%, attained at point 30. Within two standard deviations points 5 and 30 still have the highest and lowest value, respectively, and the uniformity can be estimated to $95.4 \pm 0.4\,\%$. If the underlying distribution is assumed to be Gaussian this gives a confidence interval of 95%. A graphical representation of the relative luminance is made in figure 6.3.

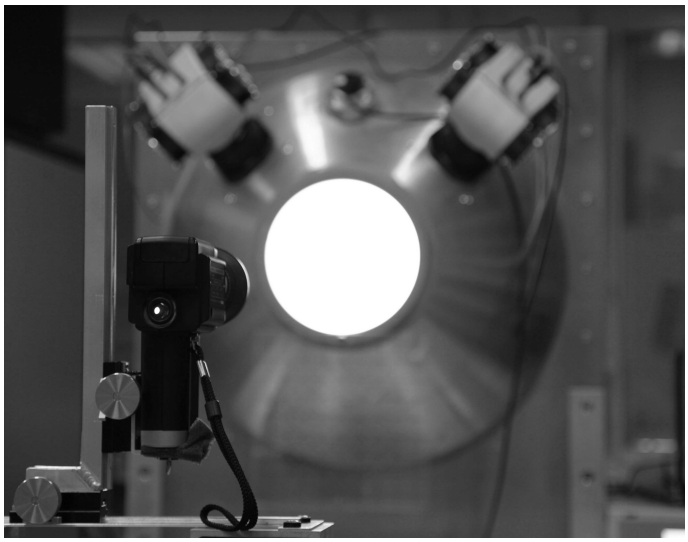

Figure 6.1: Uniformity mapping setup.

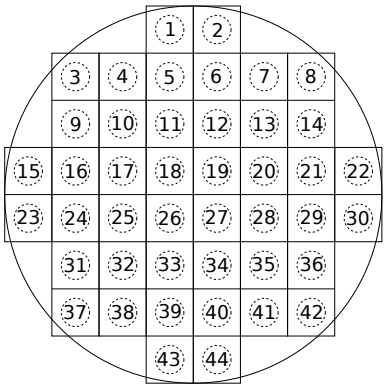

Figure 6.2: Distribution of luminance mapping points.

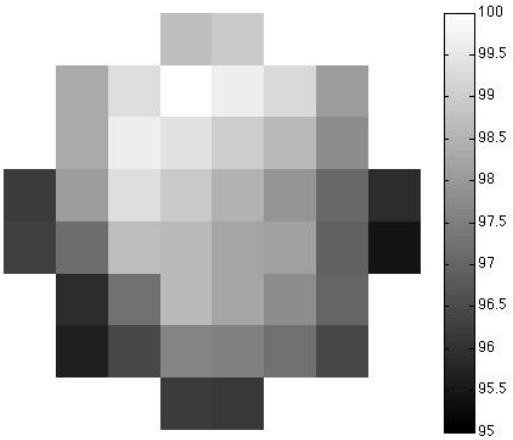

Figure 6.3: Relative luminance, %.

Table 6.1: Mean luminance, L_v, and standard deviation, σ, for the measurement points shown in figure 6.2. Based on five separate luminance mappings.

point	L_v [cd · m^{-2}]	σ [cd · m^{-2}]	point	L_v [cd · m^{-2}]	σ [cd · m^{-2}]
1	4318	10.2	23	4210	8.2
2	4330	14.6	24	4250	6.9
3	4301	7.6	25	4317	6.8
4	4345	5.4	26	4315	7.4
5	4374	3.6	27	4298	5.9
6	4360	4.5	28	4295	6.9
7	4342	7.4	29	4240	5.0
8	4289	3.0	30	4175	4.8
9	4300	4.0	31	4193	8.3
10	4360	7.1	32	4254	3.9
11	4348	7.2	33	4314	4.7
12	4332	6.6	34	4299	4.8
13	4315	6.1	35	4275	5.3
14	4277	6.8	36	4243	7.7
15	4209	5.6	37	4186	7.7
16	4291	5.4	38	4220	5.5
17	4345	7.0	39	4271	5.5
18	4329	5.2	40	4268	5.9
19	4308	8.1	41	4251	2.9
20	4284	4.4	42	4217	8.3
21	4245	4.6	43	4209	4.2
22	4195	7.6	44	4204	5.4

Table 6.2: Mean relative luminance, $L_{v,rel}$, and standard deviation, σ, for the measurement points shown in figure 6.2. Based on five separate luminance mappings.

point	$L_{v,rel}$ [%]	σ [%]	point	$L_{v,rel}$ [%]	σ [%]
1	98.72	0.23	23	96.26	0.19
2	98.98	0.33	24	97.15	0.16
3	98.33	0.17	25	98.69	0.16
4	99.34	0.12	26	98.64	0.17
5	100	0.08	27	98.27	0.14
6	99.68	0.10	28	98.20	0.16
7	99.27	0.17	29	96.94	0.11
8	98.06	0.07	30	95.44	0.11
9	98.30	0.09	31	95.86	0.19
10	99.67	0.16	32	97.25	0.09
11	99.41	0.16	33	98.63	0.11
12	99.04	0.15	34	98.28	0.11
13	98.64	0.14	35	97.74	0.12
14	97.77	0.16	36	97.01	0.18
15	96.22	0.13	37	95.70	0.18
16	98.10	0.12	38	96.47	0.12
17	99.33	0.16	39	97.65	0.13
18	98.97	0.12	40	97.57	0.13
19	98.49	0.19	41	97.19	0.07
20	97.95	0.10	42	96.41	0.19
21	97.05	0.11	43	96.23	0.10
22	95.90	0.17	44	96.11	0.12

6.1.2 Uniformity measurements with DSLR camera

To further investigate the uniformity some measurements were performed with the DSLR camera with a method described in [10]. An image was acquired of the sphere port and saved in the raw format of the camera. In the raw image the gamma compression was cancelled and the pixel values were converted from the sRGB colorspace to relative luminance with the transformation

$$Y = 0.2126 \cdot R + 0.7152 \cdot G + 0.0722 \cdot B \tag{6.1}$$

where Y is the relative luminance and R, G and B are the pixel values of the red, green and blue channel in the original image. More information on gamma compression and colorspaces can be found in [11]. All shots were taken with an ISO setting of 100 to minimize sensor noise and the exposure time, t, was chosen as high as possible without overexposing the brightest points in the image. To correct for distortions introduced by the camera a reference image was taken with the lens placed at the port of the SphereOptics-sphere. This provides the lens with uniform and diffuse light and any non-uniformities in the resulting image are introduced by the camera. The reference image can then be used to correct the original image.[4] Note that the reference image must be taken with the same aperture and focal settings as the original image in order not to change the lens geometry. Since the SphereOptics-sphere is not perfectly uniform, and because distortions of a more random nature are not removed from the images, these measurements are supposedly less accurate than the luminance mapping above.

In a first measurement the camera was placed about 2 m from the sphere port. It was equipped with a 200 mm lens and the aperture value was set to $f/4$. At this distance the rays reaching the lens are almost parallel and the resulting field of view into the sphere is small, close to the situation in the luminance mapping. In figure 6.4 the resulting relative luminance is shown, the pixels are colored in shades of gray according to their relative luminance with all pixels below 90% being black. Comparing this image to figure 6.3 the general pattern looks similar, with the darkest areas situated at the lower left and far right of the port opening.

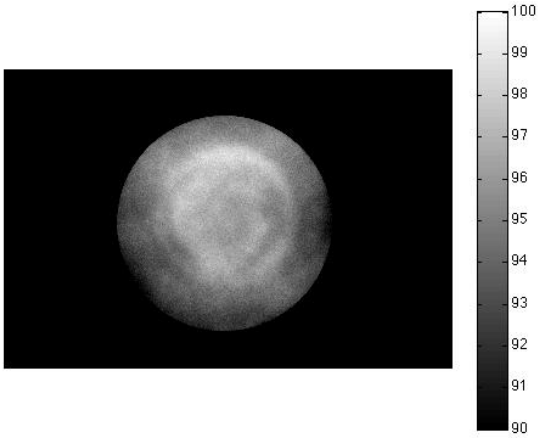

Figure 6.4: Relative luminance, %, f=200 mm, f/4, t=1/200 s.

[4] It is possible to correct for some distortions such as vignetting in the image processing software supplied with the camera. This was tried on some images and gave similar results, however the method using reference images was judged to be more trustworthy.

With the current lamp arrangement the back wall of the sphere is directly illuminated, through the diffuser glasses, and some of the radiation escaping the exit port has only been reflected once, which can lead to non-uniformities in the luminance. To investigate the effect of the lamps one of the diaphragms was completely closed so that the sphere was illuminated by one lamp at the time, figure 6.5. Although there are some minor differences in the two images the general pattern is the same, indicating that irregularities in the sphere surface and coating are responsible for most of the variations in the luminance.

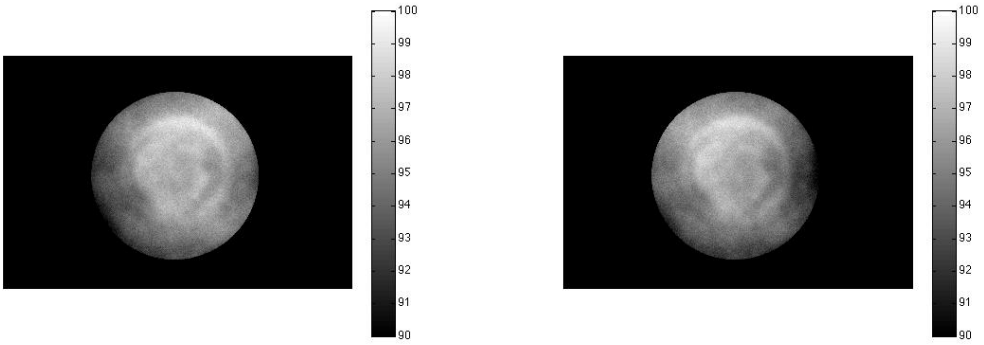

Figure 6.5: Relative luminance, %, f=200, f/4, t=1/100 s. Left and right diaphragm closed, respectively.

Figure 6.6 shows the resulting image when the aperture was set to f/32, here the grainy structure of the coating are starting to be resolved, leading to a much lower luminance uniformity.

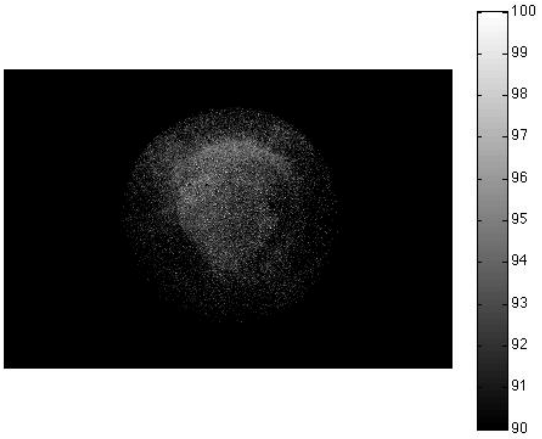

Figure 6.6: Relative luminance, %, f=200 mm, f/32, t=0.3 s.

In figure 6.7 the camera was placed at a distance of about 30 cm from the port and equipped with a 35 mm lens, f/4. The greater field of view into the sphere results in considerably lower uniformity.

In these measurements the camera was placed at some distance from the sphere, with the focal plane at the exit port. When the sphere is actually used as a light source the imaging instrument under test is usually placed close to the port, to cover the entire aperture with uniform light, and the focal plane can be chosen quite arbitrarily, often it is at infinity. Figures 6.8 and 6.9 shows some representative light rays for these two cases.

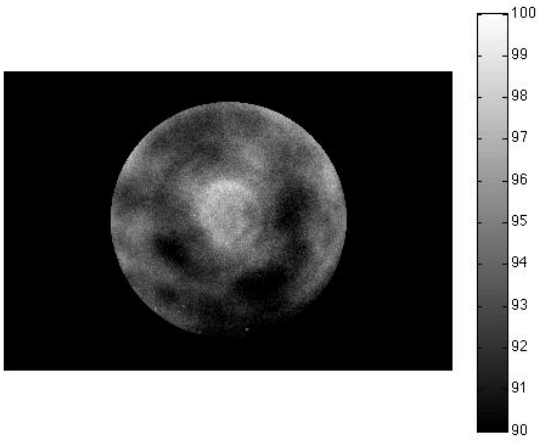

Figure 6.7: Relative luminance, %, f=35 mm, f/4, t=1/200 s.

It can be seen, for both cases, that each image point corresponds to an area of the sphere wall that decreases with decreasing aperture of the system. If the aperture is small enough the sphere wall is starting to be resolved by the imaging system which can lead to lower uniformity, as in figure 6.6. A larger field of view of the system allows the imaging system to see a larger total area of the sphere wall in both cases, also possibly leading to reduced uniformity, see figure 6.7.

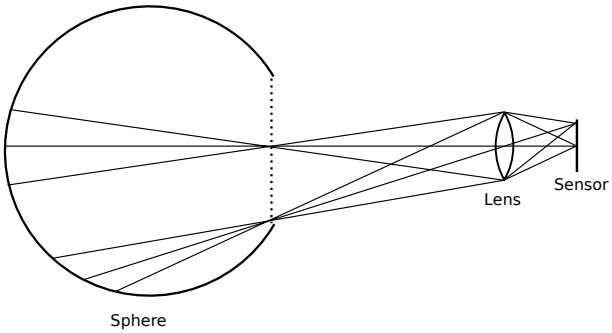

Figure 6.8: Some representative rays, imaging instrument focused at sphere port.

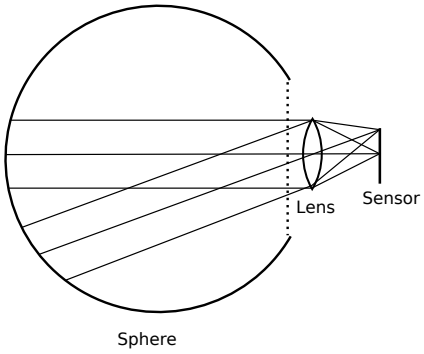

Figure 6.9: Some representative rays, imaging instrument focused at infinity.

6.2 Spectral radiance

6.2.1 Measurements with Avantes spectrometer

A first measurement of the spectral radiance was made with the diffusor at the fiber end placed directly at the sphere exit port. In this case the fiber receives flux over the full hemisphere and, assuming that the radiation from the sphere is really Lambertian, the spectral radiance of the sphere is $L_{e,\lambda} = E_{e,\lambda}/\pi$, where $E_{e,\lambda}$ is the spectral irradiance measured by the spectrometer. The resulting spectral radiance from this measurement is shown in figure 6.10. Although the full wavelength interval of the spectrometer is from 200 nm to 1100 nm the spectrum was too noisy to be useful below 300 nm and above 1000 nm. The sensitivity of the spectrometer is much lower at the ends of the interval than in the middle and consequently the calibration transfer function, that relates the signal from the spectrometer to the irradiance, is much higher. Any noise from the spectrometer is thereby amplified greatly near the ends of the wavelength interval.

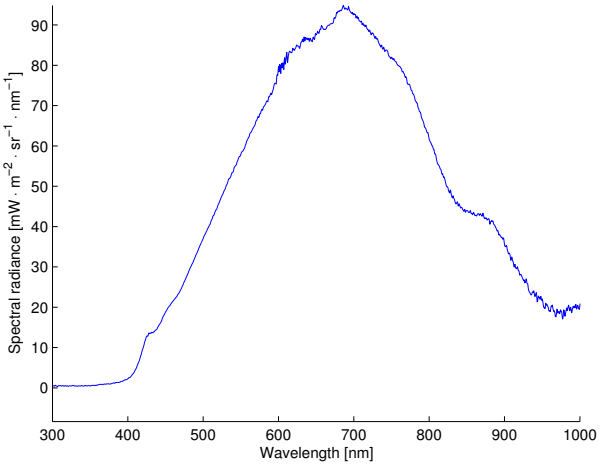

Figure 6.10: Spectral radiance, fiber end placed at sphere port.

A problem with placing the fiber end directly at the port is that it views the entire interior of the sphere, including the lamps, rendering the assumption that the radiation is Lambertian less valid. To get a smaller field of view into the sphere, more representative of what an imaging instrument would see, the fiber end can be placed at some distance from the port. Moving the fiber away from the port, however, makes the total flux received much smaller, increasing the sensitivity to stray light and noise within the spectrometer. In a second measurement the fiber was placed at a distance of 40 cm from the port, which was the greatest distance at which a reasonably good reading from the spectrometer could be acquired. Since the receiving area of the diffusor at the fiber end is much smaller than the sphere port, equation (2.15) can be used to relate the measured spectral irradiance, $E_{e,\lambda}$, to the port spectral radiance, $L_{e,\lambda}$. Dividing by dA_1 and rearranging gives

$$L_{e,\lambda} = \frac{1}{\pi}\frac{h^2 + r^2}{r^2}, \tag{6.2}$$

where h is the distance from the port and r the port radius. Figure 6.11 shows the resulting spectral radiance from the second measurement. Compared to figure 6.10 the radiance is slightly lower and contains a lot of noise above 800 nm, the spike around 890 nm is probably due to some ambient radiation. The measurements were made in a dark room and before every measurement a dark spectrum was saved and later subtracted from the measured

spectrum with the sphere turned on, however some disturbances from ambient sources can still remain.

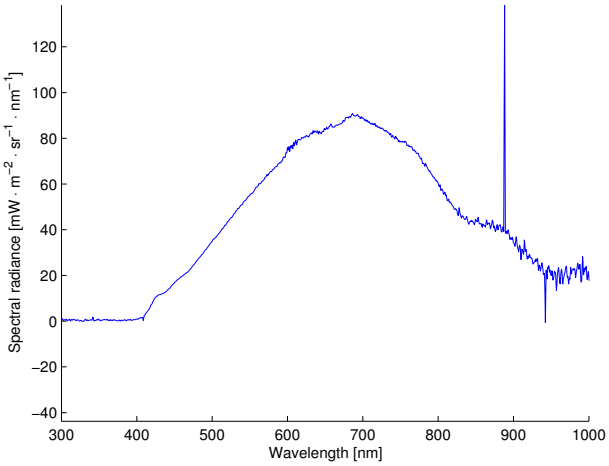

Figure 6.11: Spectral radiance, fiber end 40 cm from sphere port.

To avoid the problems associated with the two measurements the spectrum in figure 6.10 was rescaled, using a least squares fit to the spectrum in figure 6.11, over the wavelength interval from 300 nm to 800 nm. Figure 6.12 shows the rescaled spectrum from the first measurement together with the spectrum from the second measurement and figure 6.13 the rescaled spectrum alone. Table 6.3 shows the integrated radiance over a few wavelength bands. Since the spectral reflectance of the sphere coating varies over the measured wavelength interval, the flux from the lamps changes its spectral distribution upon reflection. This could lead to slightly different spectral distributions in the two measurements, however, from the good match of the curves in figure 6.12 this effect is likely to be very small. The lamps on the sphere are fitted with dichroic reflectors, that do not reflect radiation of longer wavelengths to give less thermal radiation in the beam. This is probably the reason for the substantial decline in the spectral radiance above 700 nm, with non-dichroic reflectors the spectral distribution would be closer to that of a 3000 K (the approximate temperature of the lamp filament) blackbody, like the distribution from the SphereOptics-sphere.

Using the values for the spectral radiance the luminance can be calculated to be 4200 cd/m^2 which is fairly close to the values attained in the luminance mapping. The internal illuminance meter in the sphere gave a value of 12000 lm/m^2, dividing this by π gives a luminance at the exit port of 3800 cd/m^2 which is about 10% lower. Considering that the internal meter sees the entire sphere wall, including both the lamps and the exit port, and the uncertainties in the measurement of the spectral radiance, see below, the discrepancy seems reasonable.

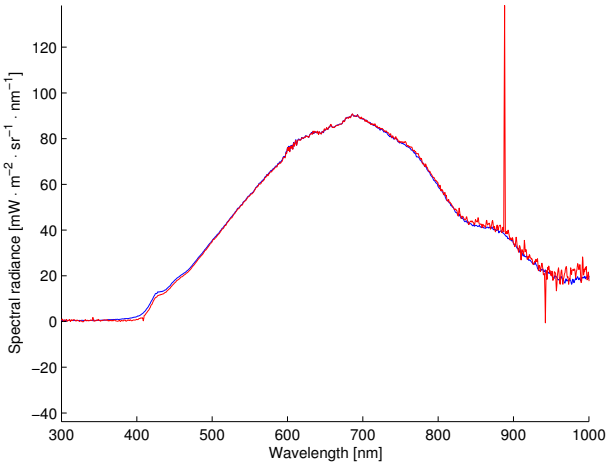

Figure 6.12: Spectral radiance with the fiber end at the sphere port, blue curve, rescaled to fit the spectral radiance with the fiber end 40 cm from the port, red curve.

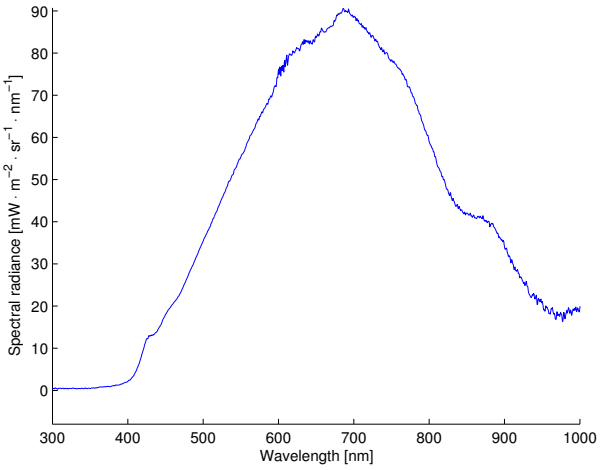

Figure 6.13: Rescaled spectral radiance, fiber end at sphere port.

Error estimation In the second measurement the uncertainty in the distance, h, from the fiber end to the sphere port is estimated to be about 5 mm. The resulting uncertainty in the calculated radiance can be estimated from (6.2) as

$$\Delta L \approx \frac{dL}{dh}\Delta h = \frac{E}{\pi}\frac{2h}{r^2}\Delta h. \tag{6.3}$$

Dividing by L and using the fact that $h = 4r$ yields

$$\frac{\Delta L}{L} \approx \frac{32}{17}\frac{\Delta h}{h}. \tag{6.4}$$

For $\Delta h = 5$ mm the resulting uncertainty in L is about 2.5%, adding the 10% uncertainty in the calibration of the spectrometer gives a total uncertainty of 12.5%. The effect of any displacement of the fiber from the normal through the center of the sphere port can be calculated from equation (2.18). For a displacement, a, of 1 cm, the difference between the configuration factors in (2.18) and (2.14), and thus the difference in the received flux, is about 0.1%. Since the uncertainty in a is much less than a centimeter this can be neglected and it also validates the approach of treating the fiber end as a differential area.

Table 6.3: Integrated radiance in a few wavelength bands.

Wavelength [nm]	Radiance $[\mathrm{mW} \cdot \mathrm{m}^{-2} \cdot \mathrm{sr}^{-1}]$
300-400	77
400-500	1800
500-600	5500
600-700	8400
700-800	7700
800-900	4400
900-1000	2200

Any angular misalignment of the fiber only adds a cosine factor to the configuration factor which can be neglected for angles up to a few degrees [12].

6.2.2 Measurements with Thorlabs detector

To get an idea of the radiance levels at longer wavelengths some measurements were performed with the Thorlabs detectors. The detectors were first placed at the port of the FOI-sphere and the signal from the detectors noted. After this the detectors were placed at the port of the SphereOptics-sphere and the radiation level was adjusted to give the same signal, the radiance could then be read off from the sphere. For these measurements to be meaningful the two spheres must have approximately the same spectral distribution over the wavelength bands of the detectors, see section 2.6, and the results should only be seen as a very rough estimation. Table 6.4 shows the integrated radiance and the mean spectral radiance obtained. The spectral radiance of the SphereOptics-sphere is only calibrated up to 2400 nm, an exponential function fitted to the interval 2000 nm to 2400 nm has been used to extrapolate values between 2400 nm and 2570 nm.

Table 6.4: Integrated radiance and mean spectral radiance from broadband measurements.

Wavelength [nm]	Integrated Radiance $[\mathrm{mW} \cdot \mathrm{m}^{-2} \cdot \mathrm{sr}^{-1}]$	Mean spectral radiance $[\mathrm{mW} \cdot \mathrm{m}^{-2} \cdot \mathrm{sr}^{-1} \cdot \mathrm{nm}^{-1}]$
1470-1750	1500	5.5
2130-2570	650	1.5

7 Conclusions and recommendations for future work

Although the measured luminance uniformity of the FOI-sphere of 95.4% is lower than most commercial spheres, with typical uniformities of 98% or better, it is still sufficient for many applications. As was shown in figure 6.7, however, this uniformity is only attained for relatively small fields of view into the sphere.

In this work the uniformity has only been measured in the visible part of the spectrum, since the sphere multiplier changes with the wavelength of the radiation the uniformity might change as well. In the measurements done in section 6.1.2, the uniformity was lowest in the blue channel if the three channels were compared before the transformation to relative luminance. This decrease in uniformity towards the blue end of the spectrum, if it is real, would be consistent with the rapid decrease in the reflectance of the coating that occurs somewhere below 500 nm, see figure 4.2. Since the uniformity of the SphereOptics-sphere, that was used as a reference in these measurements, might also vary with the wavelength, these results are not very conclusive and further investigations would be needed.

When the sphere halves was fabricated it resulted in some shallow radial grooves that could explain the circular patterns in the images in section 6.1.2. A refinishing of the sphere wall to get rid of these grooves would probably enhance the uniformity to some extent. Using a higher reflectance coating would increase both the uniformity and the maximum radiance of the sphere. To increase the uniformity even higher it might be necessary to alter the arrangement of the lamps and introduce baffles.

References

[1] EMVA Standard 1288, November 2010. URL www.emva.org.

[2] Eugene Hecht. *Optics*. Addison Wesley, fourth edition, 2002.

[3] Fred E. Nicodemus. Self-study manual on optical radiation measurements. Technical note 910-1, National Bureau of Standards, 1976.

[4] Fred E. Nicodemus. Radiance. *American Journal of Physics*, 31(5):368–377, 1963.

[5] *The Basis of Physical Photometry*. Commission Internationale de l'Eclairage, 1983.

[6] Robert Siegel & John R. Howell. *Thermal Radiation Heat Transfer*. Taylor & Francis, third edition, 1992.

[7] Labsphere Inc. *A Guide to Integrating Sphere Theory and Applications*.

[8] David G. Goebel. Generalized integrating-sphere theory. *Applied Optics*, 6(1), January 1967.

[9] *Integrating Sphere Design and Applications*. SphereOptics LLC, 2007.

[10] Felix Poulin & Maxime Caron. Display measurement - a simple approach to small-area luminance uniformity testing, 2009. URL www.ebu.ch/fr/technical/trev/trev_2009-Q2_DisplayMeasurements_CBC.pdf.

[11] Charles Poynton. *Digital Video and HDTV Algorithms and Interfaces*. Morgan Kaufmann Publishers, 2003.

[12] John R. Howell. A catalog of radiation heat transfer configuration factors. URL www.engr.uky.edu/rtl/Catalog/.

Appendix

A Solid angles

The solid angle subtended at a point P by some object is defined as the area of that object's projection onto a unit sphere with its center at P, figure A.1. The SI unit of solid angle is the steradian, [sr], which is dimensionless.

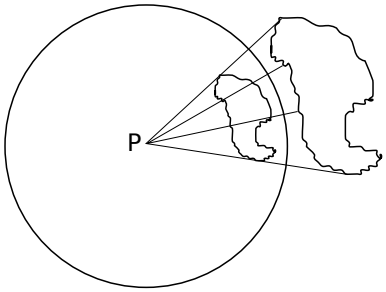

Figure A.1: Illustration of solid angle.

In spherical coordinates the element of area is $dA = r^2 \sin\theta d\theta d\phi$, figure A.2, on the unit sphere $r = 1$ and the element of solid angle is

$$d\omega = \sin\theta d\theta d\phi. \tag{A.1}$$

From the above the element of solid angle can also be written as $d\omega = dA/r^2$ where r is the distance from P to dA. Here dA must be perpendicular to the line from P to dA, if the normal to dA makes an angle θ to that line, then

$$d\omega = dA\cos\theta/r^2. \tag{A.2}$$

The solid angle subtended at its apex by a right circular cone can be calculated as

$$\omega = \int_0^{2\pi}\int_0^{\alpha} \sin\theta d\theta d\phi = 2\pi(1-\cos\alpha), \tag{A.3}$$

where α is half the planar angle subtended by the cone at its apex, figure A.3. For $\alpha = \pi/2$, $\omega = 2\pi$ which is the solid angle subtended by the hemisphere.

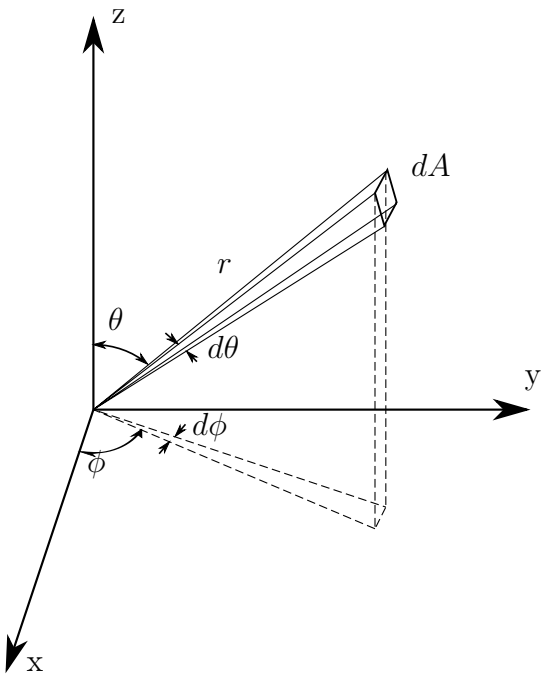

Figure A.2: Area element in spherical coordinates.

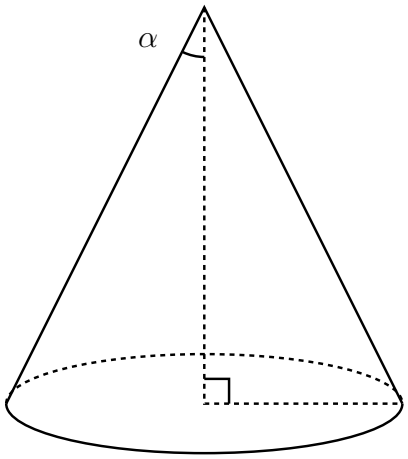

Figure A.3: Right circular cone.